Accepted Manuscript

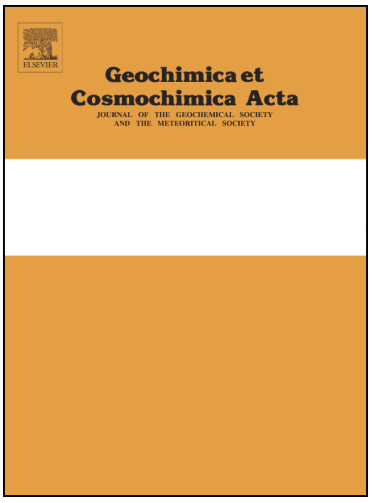

Mg isotope systematics during magmatic processes: inter-mineral fractionation in mafic to ultramafic Hawaiian xenoliths

A. Stracke, E.T. Tipper, S. Klemme, M. Bizimis

PII: S0016-7037(18)30071-1
DOI: https://doi.org/10.1016/j.gca.2018.02.002
Reference: GCA 10644

To appear in: *Geochimica et Cosmochimica Acta*

Received Date: 2 May 2017
Accepted Date: 2 February 2018

Please cite this article as: Stracke, A., Tipper, E.T., Klemme, S., Bizimis, M., Mg isotope systematics during magmatic processes: inter-mineral fractionation in mafic to ultramafic Hawaiian xenoliths, *Geochimica et Cosmochimica Acta* (2018), doi: https://doi.org/10.1016/j.gca.2018.02.002

Mg isotope systematics during magmatic processes: inter-mineral fractionation in mafic to ultramafic Hawaiian xenoliths

Stracke, A. [1,2], Tipper, E. T. [1,3], Klemme, S. [2], and Bizimis, M. [4]

[1] Institute of Isotope Geochemistry and Mineral Resources, ETH Zurich, Clausiusstrasse 25, 8092 Zurich, Switzerland.

[2] Institut für Mineralogie, Westfälische Wilhelms Universität, Corrensstrasse 24, 48149 Münster, Germany.

[3] Department of Earth Sciences, University of Cambridge, Downing Street, Cambridge, CB2 3EQ, UK

[4] School of Earth, Ocean, and Environment, University of South Carolina, 701 Sumter St., EWSC 617, Columbia, SC, 29208 USA.

Corresponding author: Andreas Stracke, Email: stracke.andreas@uni-muenster.de

Abstract

Observed differences in Mg isotope ratios between bulk magmatic rocks are small, often on a sub per mill level. Inter–mineral differences in the $^{26}Mg/^{24}Mg$ ratio (expressed as $\delta^{26}Mg$) in plutonic rocks are on a similar scale, and have mostly been attributed to equilibrium isotope fractionation at magmatic temperatures. Here we report Mg isotope data on minerals in spinel peridotite and garnet pyroxenite xenoliths from the rejuvenated stage of volcanism on Oahu and Kauai, Hawaii. The new data are compared to literature data and to theoretical predictions to investigate the processes responsible for inter–mineral Mg isotope fractionation at magmatic temperatures. Theory predicts up to per mill level differences in $\delta^{26}Mg$ between olivine and spinel at magmatic temperatures and a general decrease in $\Delta^{26}Mg_{olivine\text{-}spinel}$ (= $\delta^{26}Mg_{olivine}$ - $\delta^{26}Mg_{spinel}$) with increasing temperature, but also with increasing Cr# in spinel. For peridotites with a simple petrogenetic history by melt depletion, where increasing depletion relates to increasing melting temperatures, $\Delta^{26}Mg_{olivine\text{-}spinel}$ should thus systematically decrease with increasing Cr# in spinel. However, most natural peridotites, including the Hawaiian spinel peridotites investigated in this study, are overprinted by variable extents of melt-rock reaction, which disturb the systematic primary temperature and compositionally related olivine–spinel Mg isotope systematics. Diffusion, subsolidus re-equilibration, or surface alteration may further affect the observed olivine–

spinel Mg isotope fractionation in peridotites, making $\Delta^{26}Mg_{olivine\text{-}spinel}$ in peridotites a difficult–to–apply geothermometer. The available Mg isotope data on clinopyroxene and garnet suggest that this mineral pair is a more promising geothermometer, but its application is restricted to garnet–bearing igneous (garnet pyroxenites) and metamorphic rocks (eclogites). Although the observed $\delta^{26}Mg$ variation is on a sub per mill range in bulk magmatic rocks, the clearly resolvable inter–mineral Mg isotope differences imply that crystallization or preferential melting of isotopically distinct minerals such garnet, spinel, and clinopyroxene should cause Mg isotope fractionation between bulk melt and residue. Calculated Mg isotope variations during partial mantle melting indeed predict differences between melt and residue, but these are analytically resolvable only for melting of mafic lithologies, that is, garnet pyroxenites. Contributions from garnet pyroxenite melts may thus account for some of the isotopically light $\delta^{26}Mg$ observed in ocean island basalts and trace lithological mantle heterogeneity. Consequently, applications for high-temperature Mg isotope fractionations are promising and diverse, and recent advances in analytical precision may allow the full petrogenetic potential inherent in the sub per mill variations in $\delta^{26}Mg$ in magmatic rocks to be exploited.

Keywords: Mg isotopes, peridotite, bulk earth, mantle, basalt.

1. Introduction

Over the past 15 years, variations in Mg isotope ratios have become an important tool for investigating Mg cycling in Earth's surface environments. Early research focused on low temperature processes because of the associated large (ca. 5‰) Mg isotope variation (e.g., Brenot et al., 2008; Galy et al., 2002; Hippler et al., 2009; Pogge von Strandmann et al., 2008a; 2008b; Shen et al., 2009; Teng et al., 2010b; Tipper et al., 2006a; 2006b; Tipper et al., 2008a; 2006c; Young and Galy, 2004).

Recently, there is a growing body of work on Mg isotopes at high temperature, sparked by the expectation that isotope ratios of Mg –the second most abundant element in the bulk silicate earth– directly mirror planetary compositions and trace global (bio)geochemical cycles. It has been shown, for

example, that there is broad overlap between different types of chondrites, lunar and martian rocks (Bourdon et al., 2010; Handler et al., 2009; Norman et al., 2006; Pogge von Strandmann et al., 2011; Schiller et al., 2010; Sedaghatpour et al., 2013; Teng et al., 2010a; Wiechert and Halliday, 2007; Young and Galy, 2004). The Earth's mantle contains ca. 99.9% of Earth's Mg. Its average Mg isotope ratio is thus representative of the bulk earth and is similar to those of meteorites (Bizzarro et al., 2011; Bourdon et al., 2010; Dauphas et al., 2010; Handler et al., 2009; Huang et al., 2011; Liu et al., 2011; Pogge von Strandmann et al., 2011; Schiller et al., 2010; Teng et al., 2010a; Xiao et al., 2013; Yang et al., 2009). Hence Mg isotope fractionation during planetary accretion and differentiation is difficult to resolve. The average Mg isotope composition of Earth's mantle (peridotite) and its derivative melts (MORB and OIB) is identical (Bourdon et al., 2010; Dauphas et al., 2010; Huang et al., 2011; Teng et al., 2010a; Teng et al., 2007). Most previous studies have therefore concluded that there is no clearly resolvable Mg isotope fractionation on a bulk sample scale during mantle melting and melt differentiation, which contrasts with observations from other major elements such as Fe (Teng et al., 2013; Weyer and Ionov, 2007; Williams and Bizimis, 2014).

In contrast, recent studies have documented clearly resolvable Mg isotope fractionation between minerals in mantle peridotites (e.g., Handler et al., 2009; Hu et al., 2016; Huang et al., 2011; Li et al., 2011; Liu et al., 2011; Pogge von Strandmann et al., 2011; Wang et al., 2016; Wang et al., 2012; Wiechert and Halliday, 2007; Xiao et al., 2013; Yang et al., 2009; Young et al., 2009). These inter–mineral Mg isotope differences in mantle peridotites (and eclogites) are generally thought to reflect equilibrium magmatic fractionation, but in some cases were attributed to metasomatism (Hu et al., 2016; Huang et al., 2011; Xiao et al., 2013; Young et al., 2009), or to diffusion (e.g., Huang et al., 2011; Oeser et al., 2015; Pogge von Strandmann et al., 2011; Sio et al., 2013). Here we report Mg isotope data on minerals in spinel peridotite and garnet pyroxenite xenoliths from the rejuvenated stage of volcanism on Oahu and Kauai, Hawaii. The new data are compared to literature data and to theoretical predictions to investigate the processes responsible for inter–mineral Mg isotope fractionation at magmatic temperatures, with a special focus on the relative roles of temperature and composition. In light of the observed inter–mineral Mg isotope differences, it would be expected that partial mantle

melting, which preferentially consumes the isotopically distinct phases clinopyroxene and garnet, may lead to resolvable differences between melt (basalt) and residue (peridotite). Indeed, Zhong et al. (2017) recently suggested that small, <0.2‰, differences in δ^{26}Mg occur during partial mantle melting, but the magnitude of this fractionation relies on the inferred isotope fractionation factor between residual source (peridotite or garnet pyroxenite) and melt. Here, we present a general model for partial melting that accounts for isotopic changes in melt composition due to variable contribution of isotopically diverse minerals to the melt. We show that partial melting of mantle peridotite does not generate resolvable Mg isotope fractionation, consistent with the general overlap in δ^{26}Mg between peridotite and basalt (Bourdon et al., 2010; Dauphas et al., 2010; Huang et al., 2011; Teng et al., 2010a; Teng et al., 2007). In contrast, melting of garnet–bearing mafic source lithologies (garnet pyroxenites) produces larger Mg isotope fractionation between source and melt. In the absence of experimentally determined mineral–melt isotope fractionation factors, however, the overall offset between bulk melt and residual rock remain uncertain, but low δ^{26}Mg at high Sm/Yb observed in some ocean island basalts hint at a possible signature of garnet pyroxenite melting, and may thus trace lithological mantle heterogeneity.

2. Samples and analytical techniques

2.1. Sample selection and systematics

Five spinel peridotite and five garnet pyroxenite xenoliths from two locations on the Hawaiian islands were analyzed. All xenoliths are found within the rejuvenated stage alkali lavas from Oahu (Honolulu Volcanics (Clague and Frey, 1982)) and Kauai, Hawaii (Koloa volcanics (Garcia et al., 2010)). Samples labeled 77SL-x or Pa-x are from the Presnal collection, the 114954-x pyroxenites are from the Jackson collection, both housed at the Smithsonian Institution, Washington (Table 1). The 07Hana-001 peridotite is from the Hanapepe location, Kauai, Hawaii. The 77SL-x samples are exceptionally fresh, while the olivines in the 007Hana-001 and Pa27 samples show minor signs of alteration. Only the cleanest minerals, free of inclusions or blemishes, were handpicked for the Mg isotope analyses.

Major, trace element, and Hf, Nd, Sr, and Os isotopes compositions of the spinel peridotites from the Salt Lake Crater (SLC) and Pali vents in Oahu have been reported by Bizimis et al. (2007; 2004), and by a series of publications for the garnet pyroxenites (Bizimis et al., 2013; Bizimis et al., 2005; Keshav and Sen, 2001; Keshav et al., 2007; Sen et al., 2010; 2011). The peridotites are either fragments of the in–situ Pacific mantle lithosphere (Sen et al., 2005), or ancient recycled oceanic lithospheric components of the plume Hawaiian source (Bizimis et al., 2007). The garnet pyroxenite xenoliths are interpreted as high–pressure (2-3 GPa) cumulates from melts erupted during the rejuvenated phase of volcanism (Bizimis et al., 2005; Sen et al., 2005). Further details on the composition and origin of the analyzed samples are discussed in the supplementary information 1. In summary, the selected Hawaiian peridotites cover almost the entire range of depletions observed in abyssal peridotites and have a wide range of isotope and trace element compositions. Hence, they are ideally suited for investigating whether there is a compositional effect on inter–mineral Mg isotope fractionation at magmatic P–T conditions. In addition, the selected garnet pyroxenites provide a unique opportunity to investigate Mg isotope variability in non–peridotitic lithologies of the oceanic mantle, and for evaluating the Mg isotope fractionation between clinopyroxene and garnet as a potential geothermometer (Huang et al., 2013).

124

125 **2.2. Analytical techniques**

126 The employed analytical techniques are identical to those described in detail in Bourdon et al. (2010)
127 and Tipper et al., (2008b), but are summarized below.

128 Powdered mineral separates were digested in a 1:1 concentrated HF-HNO_3 mixture for a minimum of
129 24 hours at ~150°C, with the exception of the spinels, which were digested under high-pressure in Parr
130 bombs in HF-HNO_3 for 3-4 days to ensure complete dissolution. Afterwards, sample solutions were
131 dried down and redissolved in 6N HCl, the latter step was repeated twice to eliminate any remaining
132 fluorides. An aliquot of these solutions containing 20 μg of Mg (<1% by weight) was evaporated and
133 dissolved in 12N HCl to be loaded on a 2 ml BioRad AG1-X8 anion column, Cl^- form, 200-400 mesh.
134 Mg was eluted in 12N HCl, and the Mg fraction was evaporated, redissolved in 0.4N HCl and loaded
135 onto a 1 ml cation exchange column (Biorad AG50W-X12). Mg was collected in 1N HCl, and this
136 column procedure was repeated to obtain a pure Mg fraction. The solutions were evaporated and
137 heated to 170°C in aqua regia for 24hrs before redissolving in 16N HNO_3 to convert to a nitric salt,
138 then evaporated, and dissolved in 2% HNO_3 at ~20 ppm, ready for final dilution immediately prior to
139 analysis. Total procedural blanks were less than 10 ng (< 0.05% of the total Mg processed).

140 Mg isotope ratios were measured on a *Nu* Plasma MC-ICPMS at IGMR, ETH Zurich, using an APEX
141 Q sample introduction system coupled to an ESI ACM membrane. The samples were aspirated using a
142 PFA nebulizer with nominal uptake of 20 μl/min, resulting in excess of 14V total beam of Mg for a
143 200 ppb solution at an actual uptake of ca. 10 μl/min. Prior to introduction of the samples into the
144 mass spectrometer, all solutions were centrifuged, and diluted to within 10% of the concentration of
145 the DSM3 reference standard (200 ppb).

146 Measurements were made using a standard bracketing protocol identical to that of Tipper et al. (2008b).
147 External reproducibility (precision) of mono-elemental standards over the 14-month period of analysis
148 was 0.095‰ (2 S.D.) for δ^{26}Mg. Based on the total number of procedural replicate analyses of both
149 mono-elemental and multi-elemental standards, the maximum 2 S.D. uncertainty was estimated as
150 0.094‰ for δ^{26}Mg and 0.052‰ for δ^{25}Mg (Bourdon et al., 2010).

3. Results

Olivine (ol) and clinopyroxene (cpx) have been analyzed in all five spinel peridotites, orthopyroxene (opx) from four of the five peridotites, and isolated spinel (sp) grains suitable for Mg isotope analyses could be recovered from three peridotite samples. Garnet (grt) and cpx have been analyzed in all five pyroxenites (Table 1, Fig. 1).

In the peridotites, the $\delta^{26}Mg$ values of the olivine, orthopyroxene and clinopyroxene are similar (Table 1 and Fig. 1), with $\delta^{26}Mg_{ol}$ = -0.24 to -0.17‰, $\delta^{26}Mg_{opx}$= -0.22 to -0.15‰, and $\delta^{26}Mg_{cpx}^{peridotite}$ = -0.32 to -0.11‰. The $\delta^{26}Mg$ values in the spinels range to more positive values with $\delta^{26}Mg_{sp}$= -0.03 to +0.07. Although the $\delta^{26}Mg$ values in clinopyroxene from peridotites and pyroxenites overlap, the $\delta^{26}Mg_{cpx}$ in the pyroxenites range to more positive values with $\delta^{26}Mg_{cpx}^{pyroxenite}$= -0.13 to +0.02. The garnets from the pyroxenites have overall the most negative $\delta^{26}Mg$ values ranging from -0.58 to -0.38‰.

Calculated bulk rock $\delta^{26}Mg$ values for the peridotites ($\delta^{26}Mg$ = -0.24 to -0.16) and pyroxenites ($\delta^{26}Mg$ = -0.26 to -0.08) are close to the average value calculated for mantle-derived rocks (peridotites and basalts: $\delta^{26}Mg$ = -0.244 ± 0.062, 2 S.D., supplementary data; (Handler et al., 2009; Hu et al., 2016; Huang et al., 2011; Li et al., 2011; Liu et al., 2011; Pogge von Strandmann et al., 2011; Wang et al., 2014; Wang et al., 2016; Wang et al., 2012; Wiechert and Halliday, 2007; Xiao et al., 2013; Yang et al., 2009; Young et al., 2009; Zhong et al., 2017). In three-isotope plots of $\delta^{25}Mg$' versus $\delta^{26}Mg$' ($\delta^{2x}Mg' = 1000*\ln((\delta^{2x}Mg+1000)/1000)$; (Young and Galy, 2004)) the Hawaiian data define a line with a slope of 0.527 ± 0.087 (r^2 = 0.994), which is within error of the slope of 0.521 expected for equilibrium isotope fractionation (Young and Galy, 2004).

173 Table 1: Mg isotope data for the Hawaiian spinel peridotites and garnet pyroxenites

Sample	Mineral	^{26}Mg	2 S.D.	^{25}Mg	2 S.D.	Δ^{25}Mg'
Spinel peridotites						
07Han001	ol	-0.21	*0.02*	-0.1	*0.03*	0.005
07Han001	cpx	-0.16	*0.01*	-0.07	*0.03*	0.008
07Han001	sp	0.07	*0.04*	0.05	*0.01*	0.015
Pa27	ol	-0.24	*0.04*	-0.12	*0.02*	0.001
Pa27	opx	-0.22	*0.06*	-0.11	*0.03*	-0.001
Pa27	cpx	-0.32	*0.03*	-0.17	*0.04*	-0.001
Pa27	sp	-0.03	*0.16*	0	*0.07*	0.009
77SL405	ol	-0.17	*0.07*	-0.08	*0.02*	0.006
77SL405	opx	-0.16	*0.1*	-0.09	*0.03*	-0.009
77SL405	cpx	-0.13	*0.11*	-0.07	*0.04*	-0.003
77SL466	ol	-0.2	*0.03*	-0.11	*0.06*	-0.003
77SL466	opx	-0.2	*0.05*	-0.12	*0.04*	-0.009
77SL466	cpx	-0.15	*0.1*	-0.08	*0.06*	-0.001
77SL466	sp	0.04	*0.03*	0.02	*0.03*	0
77SL470	ol	-0.22	*0.04*	-0.11	*0.02*	0.005
77SL470	opx	-0.15	*0.06*	-0.09	*0.02*	-0.012
77SL470	cpx	-0.11	*0.02*	-0.06	*0.01*	0.001
Garnet pyroxenites						
77SL582	cpx	-0.1	*0.03*	-0.05	*0.04*	-0.001
77SL582	grt	-0.52	*0.07*	-0.27	*0.06*	-0.001
77SL620	cpx	0	*0.19*	0	*0.08*	-0.004
77SL620	grt	-0.38	*0.09*	-0.2	*0.02*	-0.004
77SL744	cpx	0.02	*0.08*	0.01	*0.02*	-0.005
77SL744	grt	-0.39	*0.03*	-0.21	*0.03*	-0.008
114954-20A	cpx	-0.03	*0.06*	-0.01	*0.02*	0.003
114954- 20A	grt	-0.42	*0.04*	-0.21	*0.04*	0.005
114954- 28A	cpx	-0.13	*0.02*	-0.05	*0.04*	0.014
114954- 28A	grt	-0.58	*0.03*	-0.29	*0.01*	0.008

174 $\Delta^{25}Mg' = \delta^{25}Mg' - 0.521 * \delta^{26}Mg'$, with $\delta^{2x}Mg' = 1000*\ln((\delta^{2x}Mg+1000)/1000)$ (Young and Galy, 2004)

175

176

177

Inter–mineral fractionation factors for the peridotite minerals $\Delta^{26}Mg_{x-y}$, calculated as $\delta^{26}Mg_x - \delta^{26}Mg_y$ –where x and y are different mineral phases– show no resolvable Mg isotope fractionation between ol and opx ($\Delta^{26}Mg_{ol\text{-}opx}$ = -0.07 to 0; Fig. 2). δ^{26}Mg values in the clinopyroxenes, however, are slightly higher than those in ol or opx (e.g., $\Delta^{26}Mg_{ol\text{-}cpx}$ = -0.11 to +0.08). Clearly resolvable, and uniform inter-mineral fractionation is observed between the spinels and other peridotite minerals (e.g., $\Delta^{26}Mg_{ol\text{-}sp}$ = -0.28 to -0.21). These inter–mineral Mg isotope fractionations are within the range of previously reported values in peridotites: $\Delta^{26}Mg_{ol\text{-}opx}$ = -0.39 to +0.07, $\Delta^{26}Mg_{ol\text{-}cpx}$ = -0.42 to +0.08, and $\Delta^{26}Mg_{ol\text{-}sp}$ = -0.88 to -0.16 (Fig. 2; (Liu et al., 2011; Wang et al., 2016; Xiao et al., 2013; Young et al., 2009)). In the pyroxenites, $\delta^{26}Mg_{grt}$ is consistently lower than $\delta^{26}Mg_{cpx}{}^{pyroxenite}$, by -0.45 to -0.38‰ ($\Delta^{26}Mg_{grt\text{-}cpx}$). This is about a factor of 2.7 less than reported for metamorphic garnet–omphacite pairs ($\Delta^{26}Mg_{grt\text{-}cpx}$ = -1.65 to -1.10) in eclogites reported by Li et al. (2011) and Wang et al. (2014) (Fig. 2), but within the range of values reported for eclogites from the South African subcontinental lithospheric mantle by Wang et al. (2012) ($\Delta^{26}Mg_{grt\text{-}cpx}$ = -0.68 to -0.38).

4. Discussion

δ^{26}Mg values in constituent minerals in peridotites and garnet pyroxenites or eclogites deviate considerably from the mantle average calculated from the available peridotite and oceanic basalt data (δ^{26}Mg = -0.245 ± 0.119, 2 S.D., n = 349; Fig. 1; supplementary data). Calculated or measured whole rock values in peridotites and garnet pyroxenites or eclogites, however, are in most cases within uncertainty of the mantle average. Inter–mineral Mg isotope variability in mantle derived rocks is thus expected to reflect temperature–dependent equilibrium isotope fractionation during magmatic processes. Especially mineral pairs with comparatively large isotopic differences, such as olivine and spinel could therefore be useful geothermometers (Liu et al., 2011; Macris et al., 2013; Schauble, 2011; Xiao et al., 2013; Young et al., 2009). However, compositional effects on inter–mineral isotope fractionation may affect the underlying temperature driven Mg isotope fractionation (e.g., Liu et al.,

2011; Macris et al., 2013; Schauble, 2011; Young et al., 2009). Additional complexity –on the mineral or whole rock scale– may be introduced by diffusion (e.g., Huang et al., 2011; Oeser et al., 2015; Pogge von Strandmann et al., 2011; Sio et al., 2013), metasomatic processes (Hu et al., 2016; Huang et al., 2011; Xiao et al., 2013; Young et al., 2009), and subsolidus re-equilibration of mineral phases. In light of these potential complications we will discuss the applicability of the two most promising mineral pairs for Mg isotope geothermometry: olivine–spinel (Liu et al., 2011; Macris et al., 2013; Schauble, 2011; Xiao et al., 2013; Young et al., 2009) and garnet–clinopyroxene. To minimize potential disequilibrium effects by natural or analytical processes, the following discussion will only use literature data where $\Delta^{25}Mg'$ indicates $\delta^{25}Mg$ and $\delta^{26}Mg$ within 3% of equilibrium (i.e., $-0.03 < \Delta^{25}Mg' < 0.03$; where $\Delta^{25}Mg' = \delta^{25}Mg' - 0.521 * \delta^{26}Mg'$ (Young and Galy, 2004)).

4.1 Inter-mineral Mg isotope fractionation in mantle rocks

4.1.1. Mg isotope fractionation between olivine and spinel

Theoretical and experimental studies predict up to per mill level Mg equilibrium isotope fractionation between olivine and spinel at magmatic temperatures, caused by differences in Mg–O bond length for the six-fold coordinated Mg^{2+} in olivine and mostly four–fold coordinated Mg^{2+} in spinel (Macris et al., 2013; Schauble, 2011). In spinels –with a general composition of AB_2O_4– theory predicts that Mg–O bond length of the tetrahedral A site depends on which cation occupies the octahedral B site (Schauble, 2011). The Mg–O bond length in $MgAl_2O_4$ (1.964Å) is shorter than in $MgCr_2O_4$ (2.001Å) (Schauble, 2011), leading to a preference for the heavy Mg isotope in $MgAl_2O_4$ relative to $MgCr_2O_4$. In addition to the general temperature dependence, therefore, $\Delta^{26}Mg_{ol\text{-}sp}$ should vary systematically with the relative amount of Cr in the octahedral B site, that is, the Cr# in spinel (Fig. 3). The theoretically predicted range in Mg–O bond lengths (1.964 – 2.001 for Cr# 0-1, (Schauble, 2011)) is on the same order as the Mg–O bond length in natural spinels (1.945 – 1.965 for Cr# 0 – 0.3; (Princivalle et al., 1989)), suggesting that theoretical predictions should also apply to natural spinels, at least qualitatively. As shown in Fig. 3a, high Cr# and high temperature for olivine–spinel equilibration predict low $\Delta^{26}Mg_{ol\text{-}sp}$.

In peridotites, the Cr# in spinel increases with the extent of melting experienced (Dick and Bullen, 1984). In absence of volatile induced, or redox partial melting, larger degrees of melting occur at higher temperatures. In this case, peridotites with increasing Cr# should reflect higher melting temperatures, and show progressively decreasing $\Delta^{26}Mg_{ol\text{-}sp}$. For peridotites with a simple petrogenetic history of melt depletion, a strong inverse coupling between $\Delta^{26}Mg_{ol\text{-}sp}$ and Cr# would thus be expected (Fig. 3a). However, few, if any of the peridotites analyzed for Mg isotope ratios preserve such a simple petrogenetic history (Fig. 4). The only likely candidate are peridotites from the North China Craton investigated by Liu et al. (2011). These rocks preserve the expected correlation between Al_2O_3 (whole rock) or Cr# in spinel with Mg# (olivine) for variably depleted residual peridotites (Fig. 4), although their rare earth element patterns also show variable metasomatic overprint (Wu et al., 2006). All other peridotite suites that include data for $\delta^{26}Mg$ in spinel have experienced considerable post–depletion metasomatism by interaction with silicate melts (Liu et al., 2011; Xiao et al., 2013; Young et al., 2009), including the Hawaiian peridotites investigated in this study (Bizimis et al., 2004). Melt–peridotite reaction incongruently dissolves pyroxenes and forms olivine, spinel, and a modified melt (Kelemen et al., 1990). Melt-rock reaction, especially at lower temperature than for the primary depletion by partial melting, can therefore disturb the primary, partial melting–related $\Delta^{26}Mg_{ol\text{-}sp}$ and Cr# signatures (Fig. 3a). Hence a first–order control by temperature on $\Delta^{26}Mg_{ol\text{-}sp}$ is difficult to establish in natural peridotites investigated for Mg isotopes thus far, because of the almost ubiquitous and variable overprint by post–melting metasomatism (e.g., Hu et al., 2016; Huang et al., 2011; Xiao et al., 2013; Young et al., 2009). Note that even for the suite of spinel peridotites from the North China Craton, the inferred temperature control on $\Delta^{26}Mg_{ol\text{-}sp}$ by Liu et al. (2011) is difficult to establish given analytical uncertainty and superimposed compositional effects due to variable Cr#, which make it difficult to assign the observed variation in $\Delta^{26}Mg_{ol\text{-}sp}$ solely to temperature (Fig. 3a).

Moreover, a discrepancy of several hundred °C is observed between temperatures predicted from $\Delta^{26}Mg_{ol\text{-}sp}$ (Schauble, 2011) and mineral equilibria (e.g., cpx–opx,(Brey and Köhler, 1990), compare Fig. 3a and b). This discrepancy is observed for the Hawaiian peridotite xenoliths, but also for the peridotites investigated previously (Liu et al., 2011; Xiao et al., 2013; Young et al., 2009), and may point

either to an offset in calculated temperatures from $\Delta^{26}Mg_{ol\text{-}sp}$, or different closure temperatures of Mg isotope exchange between olivine and spinel relative to Fe–Mg exchange between orthopyroxene and clinopyroxene (Brey and Köhler, 1990; Wells, 1977). It should also be considered that, owing to the shallow slope of the predicted $\Delta^{26}Mg_{ol\text{-}sp}$ – temperature curves (Fig. 3b; (Macris et al., 2013; Schauble, 2011)), the uncertainties in predicted temperatures from Mg isotope variations are several hundred °C at temperatures >1000°C, assuming an uncertainty of ± 0.10‰ (2 S.D.) on $\delta^{26}Mg_{ol}$ and $\delta^{26}Mg_{sp}$, and thus a propagated uncertainty on $\Delta^{26}Mg_{ol\text{-}sp}$ of ± 0.14‰ (2 S.D.). For current analytical uncertainties, therefore, temperatures predicted from $\Delta^{26}Mg_{ol\text{-}sp}$ are less precise, and may also be less accurate than those derived from conventional mineral–mineral thermometers (e.g., (Roeder et al., 1979; Wan et al., 2008)), although different geothermometers may also diverge by over 200°C, even in well-equilibrated peridotite and pyroxenite mantle xenoliths (Nimis and Grütter, 2010).

4.1.2 Mg isotope fractionation between garnet and clinopyroxene

Mg occupies the 8–fold coordinated A site in garnet with a general formula $A_3B_2Si_3O_{12}$. The 3+ cations Fe, Al, and Cr occupy the octahedral B site in garnet. Huang et al. (2013) inferred from theory that Mg–O bond length, and thus Mg isotope fractionation in garnet, is largely insensitive to variable cation composition on both the A and B sites, and could thus serve as a thermobarometer (Huang et al., 2013).

For the eclogites studied by Wang et al. (2012), which are interpreted as metamorphosed altered oceanic crust, temperatures estimated from Fe-Mg exchange in clinopyroxene–garnet (Ellis and Green, 1979) and those predicted by $\Delta^{26}Mg_{cpx\text{-}grt}$ (Huang et al., 2013) agree within uncertainty (Fig. 5). The eclogites from the Dabie orogen investigated by Li et al. (2011) are ultra-high-pressure (UHP) metamorphic eclogites with gabbroic protoliths. The temperatures estimated from $\Delta^{26}Mg_{cpx\text{-}grt}$ (Huang et al., 2013) for these samples are 100-200°C higher than the Fe–Mg exchange temperatures (549–614°C). At these low temperatures, uncertainties in predicted temperatures are little influenced by the analytical uncertainty on $\Delta^{26}Mg_{cpx\text{-}grt}$ (± 0.14‰, see above) and are ca. ~50-70°C, (Fig. 5a). Hence the observed discrepancy likely arises from uncertainties in estimating Fe^{3+} contents from Fe_{total} in these

mineral phases, which leads to anomalously low Fe–Mg exchange temperatures well outside the calibrated temperature range of this empirical thermobarometer (Ellis and Green, 1979).

The Hawaiian garnet pyroxenites analyzed in this study are interpreted as high–pressure (2-3 GPa) cumulates from melts erupted during the rejuvenated phase of volcanism (Bizimis et al., 2005; Sen et al., 2005). The temperatures of last equilibration estimated from Fe–Mg exchange (Bizimis et al., 2005) and Mg isotope fractionation for three out of five Hawaiian samples are within 40–80°C, and therefore considered in good agreement. The other two samples show larger deviations: 140 and 260°C, respectively. The largest difference of 260°C is for sample 77SL-620 with a T ~1160°C based on Fe–Mg exchange (Bizimis et al., 2005), but a T ~ 1420°C based on $\Delta^{26}Mg_{cpx\text{-}grt}$ = 0.38 (Table 1, Fig. 5). Although a seemingly large difference, it should be considered that uncertainties of ± 0.14‰ on $\Delta^{26}Mg_{cpx\text{-}grt}$ (see above) translate into uncertainties in temperature of ~150–250°C at T ~1200°C (Fig. 5a). Considering analytical uncertainties on $\Delta^{26}Mg_{cpx\text{-}grt}$, temperatures estimated from Fe-Mg exchange and $\Delta^{26}Mg_{cpx\text{-}grt}$ therefore mostly agree within uncertainty (Fig. 5a).

4.2 Bulk rock Mg isotope fractionation during magmatic processes

Mantle–derived rocks (i.e., peridotites, basalts) exhibit a small range in δ^{26}Mg from -0.48 to about 0 (Fig. 6; supplementary data). The global averages of peridotites (δ^{26}Mg = -0.243‰ ± 0.135, 2 S.D., n = 184), mid ocean ridge basalts (MORB; δ^{26}Mg = -0.239‰ ± 0.102, 2 S.D., n = 74) and ocean island basalts (OIB; δ^{26}Mg = -0.252‰ ± 0.096, 2 S.D., n = 91) are identical within uncertainty and have similar variance (supplementary figure 2). Accordingly, previous studies have concluded that neither partial melting nor crystal fractionation significantly affect the Mg isotope variability of oceanic basalts on the bulk sample scale (Bourdon et al., 2010; Dauphas et al., 2010; Huang et al., 2011; Teng et al., 2010a; Teng et al., 2007). Magmatic differentiation at shallow depths (< 1 GPa) in basaltic melts dominantly involves phases whose Mg isotope composition is similar to that of the bulk rock (olivine, Fig. 1), or phases that contain little Mg (plagioclase). Thus, fractional crystallization of basaltic melts does not produce significant Mg isotope fractionation (e.g., Teng et al., 2007), unless large amounts of clinopyroxene with slightly different Mg isotope composition compared to the bulk rocks (Fig. 1)

dominate the fractionating assemblage. Partial melting in Earth's mantle, however, preferentially consumes clinopyroxene and garnet, which have δ^{26}Mg significantly different from the average bulk mantle (Fig. 1), and may therefore induce isotopic differences between melt (basalt) and residue (peridotite) (Zhong et al., 2017). If so, this needs to be reconciled with the identical average δ^{26}Mg of basalts and peridotites.

In the following, Mg isotope fractionation during partial melting of mantle lithologies is investigated using an incremental non-modal melting model, equivalent to fractional melting (Shaw, 1970). For details of the modeling see the supplementary information. In the absence of experimentally determined mineral–melt isotope fractionation factors, $\alpha_{\text{mineral-melt}}$, these can be estimated from known inter–mineral isotope fractionation factors (Fig. 2), and one known or estimated $\alpha_{\text{mineral-melt}}$ (cf. Williams and Bizimis, 2014; Zhong et al., 2017) as a reference point. Olivine and orthopyroxene are isotopically almost identical to bulk peridotite and basaltic melts, and thus have $\alpha_{\text{ol,opx-melt}} \sim 1$ (Fig. 1, 2, and supplementary figure 2). Moreover, Mg occurs in five to six–fold coordination in silicate melts (George and Stebbins, 1998; Shimoda et al., 2007), similar to Mg in olivine and orthopyroxene, providing additional support for the assumption that little, if any, isotope fractionation between olivine or orthopyroxene and melt occurs. Alternatively, minimum $\alpha_{\text{mineral-melt}}$ can be calculated from known inter–mineral isotope fractionation factors (Fig. 2) and assuming an initial $\alpha_{\text{source-melt}} = 1$, which appears reasonable for Mg, because peridotites and basalts have, on average, almost identical δ^{26}Mg (Fig. 1, supplementary figure 2). The latter approach anchors the initial melt at the initial $^{26}Mg/^{24}Mg$ of the residue (initial $\alpha_{\text{source-melt}} = 1$, Fig. 7), but would offset the initial $^{26}Mg/^{24}Mg$ of the melt from its source for $\alpha_{\text{source-melt}} \neq 1$. The former approach for calculating initial $\alpha_{\text{source-melt}}$ offsets the initial $^{26}Mg/^{24}Mg$ of the melt to that of the peridotite source proportional to the difference between the $^{26}Mg/^{24}Mg$ of olivine (orthopyroxene) and the bulk peridotite. For melting garnet pyroxenite sources, $\alpha_{\text{cpx,grt-melt}}$ can

also be calculated from known inter–mineral isotope fractionation factors (Fig. 2) and assuming $\alpha_{source-melt} = 1$, or, $\alpha_{cpx,grt-melt}$ similar to those derived for peridotite–melt can be used. Similar to the peridotite case, the initial melt is either anchored or slightly offset from the initial $^{26}Mg/^{24}Mg$ of the garnet pyroxenite. It should be stressed that the inherent assumptions for calculating $\alpha_{source-melt}$ are critical for assessing the overall isotopic offset between source and melt (cf. Williams and Bizimis, 2014; Zhong et al., 2017). Importantly, the magnitude of isotope fractionation between source and melt remains uncertain in the absence of experimentally determined $\alpha_{mineral-melt}$, but the relative changes in $^{26}Mg/^{24}Mg$ ($\delta^{26}Mg$) of melt and residue with progressive melting are independent of their initial values and are thus a robust feature for any given melting scenario. The following discussion of the effect of partial melting on the $\delta^{26}Mg$ of the derivative melts will therefore focus on these relative changes in $\delta^{26}Mg$ with progressive melting. In Fig. 6, all $\alpha_{mineral-melt}$ are estimated assuming the initial $\alpha_{source-melt} = 1$, hence are initially anchored at their source value, but it should be kept in mind that larger offsets between melt and residue would occur for initial $\alpha_{source-melt} \neq 1$.

Figure 6 shows that for melting garnet peridotite at high P-T (OIB melting), melts evolve to slightly lower $\delta^{26}Mg$ compared to their initial value, but only by < 0.01‰. The changing $\delta^{26}Mg$ of the partial melts with increasing extent of melting (F) reflect the changing contribution of Mg of each mineral to the melt. For the melt reactions assumed here, formation of orthopyroxene, and consumption of clinopyroxene and garnet characterize the melting of garnet peridotite at high P and low F. During this early stage of melting, clinopyroxene delivers approximately four times more Mg to the melts than garnet, thus outweighs the effect of melting garnet with $\delta^{26}Mg$ lower than the bulk peridotite. During the rapid transition from garnet to spinel peridotite, spinel (and orthopyroxene) is formed at the expense of garnet (and olivine) and a large amount of Mg from garnet enters the melt, thus decreasing its $\delta^{26}Mg$. Eventually, after garnet disappears from the residue, almost only clinopyroxene delivers Mg

358 to the produced melt, which slightly increases the δ^{26}Mg in the incremental melts. During melting of
359 peridotite at comparatively lower P-T (MORB melting), garnet is residual only during the initial stages,
360 or absent from the residual assemblage. In this latter case, melting is dominated by clinopyroxene, and
361 the δ^{26}Mg of the produced melts increase in δ^{26}Mg, but still remains within <0.01‰ of its starting value
362 (Fig. 6). Overall, partial melting of peridotite therefore does not produce resolvable Mg isotope
363 variation, unless the assumption inherent in calculating $\alpha_{source\text{-}melt}$ lead to values substantially different
364 from 1 (cf. Zhong et al., 2017). The reason is that the $\alpha_{source\text{-}melt}$ is buffered ~ 1 by residual olivine and
365 orthopyroxene, which together host ca. 90% of the Mg and have $\alpha_{ol,opx\text{-}melt}$ ~ 1 (Fig. 1).

366 More significant Mg isotope fractionation during partial melting is expected only if the predominant
367 contribution of Mg is from phases with δ^{26}Mg significantly different from that of the bulk rock. Melting
368 of mafic lithologies, such as garnet pyroxenite, imposes a pronounced garnet signature onto the
369 derivative melts, and thus results in δ^{26}Mg variability in excess of that for peridotite melting (Fig. 6).
370 Melts of G2 pyroxenite are dominated by melting garnet at low extent of melting, but are increasingly
371 dominated by melting clinopyroxene with progressive extent of melting (Pertermann and Hirschmann,
372 2003a, b). Owing to the persistent strong garnet influence, the δ^{26}Mg of garnet pyroxenite melts remains
373 lower than their starting value, by ca. 0.03–0.04‰, even for extents of melting >50% (Fig. 6). However,
374 the δ^{26}Mg of garnet pyroxenite melts strongly depend on the relative contribution of Mg from
375 clinopyroxene and garnet. Below ca. 12% of melting, garnet delivers more Mg to the melt than
376 clinopyroxene, which is reversed at F > 12% (Fig. 6), and garnet pyroxenite melts then deviate less from
377 that of the bulk residue, similar to what is observed for peridotite-derived melts.

378 In the OIB investigated thus far, the lowest δ^{26}Mg in OIB occur in rocks with the highest Sm/Yb
379 and tend to decrease with increasing Sm/Yb (Fig. 7). This observation is consistent with the greater
380 influence of residual garnet during melting predicted by our model. Some scatter is induced by variable
381 amounts of clinopyroxene accumulation or fractionation (Fig. 7), but the available data hint at a
382 possible decrease of δ^{26}Mg with progressively lower degrees of melting in the garnet–stability field, that

383 is, higher Sm/Yb (Fig. 7). As discussed above, δ^{26}Mg significantly lower than their initial source are only
384 expected for melting garnet pyroxenite, and this observation could therefore be indicative of an
385 increasing garnet pyroxenite melt component in OIB with increasingly lower δ^{26}Mg. Confidently
386 resolving this effect, however, would require larger absolute values of $\alpha_{\text{mineral-melt}}$ than the minimum
387 values assumed for the modeling in this study, or, alternatively more precise Mg isotope data (see
388 discussion above and Fig. 7). Whereas the data for Hawaiian alkali basalts compared to tholeiites by
389 Zhong et al. (2017) are compatible with such an interpretation, the data for Hawaiian tholeiites reported
390 previously (Teng et al., 2010a) do not show any systematic variation in Figure 7. Although this
391 observation is consistent with the small variability of Sm/Yb and δ^{26}Mg at the similarly large degrees of
392 melting expected for Hawaiian tholeiites, significant analytical uncertainty in the δ^{26}Mg and the trace
393 element data compiled for the Hawaiian tholeiites (see Fig. 7 and supplementary data) –but also
394 variable amounts of clinopyroxene fractionation– may obscure an inherent systematic relationship as
395 observed by Zhong et al. (2017). In MORB (including Iceland) the invariably low Sm/Yb reflect large
396 amounts of melting in the spinel–stability field (Fig. 6 and 7). δ^{26}Mg in MORB scatter around the
397 MORB average (-0.239‰ ± 0.102, S.D., n = 74; supplementary data), probably mostly due to analytical
398 uncertainty in δ^{26}Mg, but some low δ^{26}Mg could also be consistent with a garnet pyroxenite melt
399 component. It should also be noted that the relatively large extents of melting for MORB and the
400 Hawaiian tholeiites make it difficult to resolve potential pyroxenite δ^{26}Mg signatures. For melting of
401 lithologically heterogeneous mantle sources, the relative contribution of pyroxenite–derived melt to the
402 erupted melt decreases with increasing extent of (peridotite) melting (c.f. Stracke and Bourdon, 2009).
403 Large overall extents of partial melting also minimize any variation in Sm/Yb, thus making it more
404 difficult to resolve correlated small differences in δ^{26}Mg in pyroxenite versus peridotite–derived melts,
405 especially in light of the current analytical uncertainty on δ^{26}Mg.
406

407 **4.3 Applications for Mg isotope fractionation during magmatic processes**

Several studies highlighted the potential application of large inter–-mineral olivine–spinel fractionation as a geothermometer in peridotites (Liu et al., 2011; Schauble, 2011; Xiao et al., 2013; Young et al., 2009). A dominant effect of temperature on $\Delta^{26}Mg_{ol\text{-}sp}$, however, can only be expected for refractory peridotites with a simple petrogeneitc history by melt depletion. In this case a superimposed compositional effect on Mg isotope fractionation in spinel, that is, decreasing $\Delta^{26}Mg_{ol\text{-}sp}$ with increasing Cr# in spinel (Fig. 3, (Schauble, 2011)), should further diminish the decreasing $\Delta^{26}Mg_{ol\text{-}sp}$ with increasing temperature. However, most of the peridotites analyzed for Mg isotopes so far do not preserve such a simple petrogenetic history, but have $\Delta^{26}Mg_{ol\text{-}sp}$ that are variably overprinted by metasomatism (melt–rock reaction, Fig. 4). A possible exception may be the peridotites from the North China Craton investigated by Liu et al. (2011). Even in this latter case, however, disentangling temperature and compositionally related effects on $\Delta^{26}Mg_{ol\text{-}sp}$ proves complicated (Fig. 3a), making olivine–spinel Mg isotope fractionation in peridotites a difficult–to–apply geothermometer. Moreover, in addition to melt–rock reaction (metasomatism) subsolidus re-equilibration, diffusion (e.g., Huang et al., 2011; Oeser et al., 2015; Pogge von Strandmann et al., 2011; Sio et al., 2013), or surface alteration may also affect the Mg isotope composition of olivine and spinel in mantle peridotites.

In contrast to olivine–spinel, inter–mineral Mg isotope fractionation between co–existing clinopyroxene and garnet (Li et al., 2011; 2014; Wang et al., 2012); and this study) is a more promising geothermometer (see also Huang et al., 2013). However, significant deviations between temperatures estimated from Mg isotope fractionation and Fe–Mg exchange between cpx and grt are observed, mostly at T<800°C, probably due to anomalously low Fe–Mg exchange temperatures resulting from uncertainties in estimating Fe^{3+}–Fe^{2+} contents (Ellis and Green, 1979). Uncertainties on temperature estimates from $\Delta^{26}Mg_{cpx\text{-}grt}$ at higher magmatic temperatures may arise mostly from analytical uncertainty in $\Delta^{26}Mg_{cpx\text{-}grt}$ (~ ± 0.14‰) which is several 100°C at T >1100–1200°C (Huang et al., 2013), Fig. 5). Precise temperature estimates based on $\Delta^{26}Mg_{cpx\text{-}grt}$ are thus only possible within a small temperature range between T~800–1100°C, restricting its use to garnet–bearing igneous and metamorphic rocks. It should also be assessed whether the potential information to be derived from Mg isotope thermobarometry warrants the substantially larger analytic effort compared to conventional Fe–Mg

exchange thermobarometers.

Applications of Mg isotope fractionation on the bulk sample scale in magmatic rocks have so far been elusive, because of the associated small range of δ^{26}Mg. Zhong et al. (2017) recently argued that partial melting leads to Mg isotope fractionation on a level of tenths of per mill. However, the observation that olivine and orthopyroxene have similar δ^{26}Mg as both average peridotite and basalts (Fig. 1, 2, and supplementary figure 2) indicates that $\alpha_{ol,\ opx\text{-}melt} \sim 1$. Given the predominance of olivine and orthopyroxene on the Mg budget of peridotite, partial melting of peridotite does not result in resolvable Mg isotope fractionation, in good agreement with the identical average δ^{26}Mg in peridotites and basalts (supplementary figure 2). More variable δ^{26}Mg may only result from melting mafic source lithologies such as garnet pyroxenite, consistent with a tendency of lower δ^{26}Mg with higher Sm/Yb (Fig. 7). At current levels of analytical precision, however, this effect is only resolvable with confidence for larger absolute values of $\alpha_{mineral\text{-}melt}$ than assumed for the modeling in this study (Fig. 6). Low δ^{26}Mg at high Sm/Yb observed in some alkaline OIB, however, hint at a possible signature of garnet pyroxenite melting, in which case δ^{26}Mg trace lithological mantle heterogeneity. In contrast, the higher extents of melting inferred for tholeiitic OIB and especially MORB, lead to much less variable Sm/Yb than in the low degree alkaline OIB, making it difficult to resolve potentially correlated sub per mill variations in δ^{26}Mg.

Owing to the general lack of offset in δ^{26}Mg between mantle sources and melt (supplementary figure 2), Mg isotope ratios in mantle–derived rocks should accurately reflect bulk planetary composition. Hence, comparison of δ^{26}Mg in meteorites and bulk planets could provide valuable information about the provenance of planet forming materials, and the processes that lead to Mg isotope fractionation during planet formation and early differentiation. However, while some earlier studies invoke a difference between silicate Earth and chondrites (Wiechert and Halliday, 2007; Young et al., 2009), most recent studies have argued for a broadly similar Mg isotope composition (Bizzarro et al., 2011; Bourdon et al., 2010; Handler et al., 2009; Huang et al., 2011; Liu et al., 2011; Schiller et al., 2010; Teng

et al., 2010a; Yang et al., 2009). A compilation of the available data yields average values of -0.270 (± 0.074, S.D., n = 102) and -0.247 (± 0.064, S.D., n = 389) for δ^{26}Mg in chondrites and terrestrial mantle–derived rocks (basalts, eclogites, and peridotites), respectively (supplementary data). As pointed out by Pogge von Strandmann et al. (2011), these averages are statistically different based on a student's t-test. Recent, more precise Mg isotope measurements have substantiated this small difference in δ^{26}Mg between chondritic meteorites and the bulk silicate Earth and attributed it to vapor loss from growing planetesimals (Hin et al., 2017).

In summary, in addition to being potential geothermometers (especially clinopyroxene–garnet), stable Mg isotope variations in magmatic rocks may be a useful tool for identifying lithological heterogeneity in the mantle. Analysis of peridotitic garnets and the investigation of specifically targeted OIB suites should allow further constraints on the potential variation in δ^{26}Mg in response to partial melting. Most crucial in this respect, however, is to determine isotope fractionation factors between mantle minerals and melt, $\alpha_{\text{mineral-melt}}$, which would determine the actual offsets in δ^{26}Mg between melt and source, and thus further constrain the respective influence of different source lithologies on the δ^{26}Mg of mantle melts. Applications for high–temperature Mg isotope fractionation are thus diverse, but further improving the analytical precision of Mg isotope measurements (e.g., Hin et al., 2017) has proven crucial for planetary scale applications, and also holds promise for investigating a diverse range of magmatic processes at higher resolution.

Acknowledgments

We would like to thank the reviewers, Jasper Konter, Merlin Méheut, and the associate editor Nicolas Dauphas for their helpful and constructive comments, which significantly improved parts of the discussion. Marc Norman is thanked for editorial handling. ETT was supported by a Marie-Curie Inter-European-Fellowship No. 41189 at ETH Zürich for research on global budgets of Ca and Mg and a Cambridge NERC Fellowship (NE/G013764/1) at the University of Cambridge. MB acknowledges NSF grants OCE-0622827 and OCE - 0852488 for sample collection and processing.

References

Bizimis, M., Griselin, M., Lassiter, J.C., Salters, V.J.M. and Sen, G. (2007) Ancient recycled mantle lithosphere in the Hawaiian plume: Osmium-Hafnium isotope evidence from peridotite mantle xenoliths. Earth Planet. Sci. Lett. 257, 259-273.

Bizimis, M., Salters, V.J.M., Garcia, M.O. and Norman, M.D. (2013) The composition and distribution of the rejuvenated component across the Hawaiian plume: Hf-Nd-Sr-Pb isotope systematics of Kaula lavas and pyroxenite xenoliths. Geochem. Geophys. Geosys. 14, doi:10.1002/ggge.20250.

Bizimis, M., Sen, G. and Salters, V.J.M. (2004) Hf-Nd isotope decoupling in the oceanic lithosphere. constraints from spinel peridotites from Oahu, Hawaii. Earth Planet. Sci. Lett. 217, 43-58.

Bizimis, M., Sen, G., Salters, V.J.M. and Keshav, S. (2005) Hf-Nd-Sr isotope systematics of garnet pyroxenites from Salt Lake Crater, Oahu, Hawaii: Evidence for a depleted component in Hawaiian volcanism. Geochim. Cosmochim. Acta 69, 2629-2646.

Bizzarro, M., Paton, C., Larsen, K., Schiller, M., Trinquier, A. and Ulfbeck, D. (2011) High-precision Mg-isotope measurements of terrestrial and extraterrestrial material by HR-MC-ICPMS-implications for the relative and absolute Mg-isotope composition of the bulk silicate Earth. Journal of Analytical Atomic Spectrometry 26, 565-577.

Bourdon, B., Tipper, E.T., Fitoussi, C. and Stracke, A. (2010) Chondritic Mg isotope composition of the Earth. Geochim. Cosmochim. Acta 74, 5069-5083.

Brenot, A., Cloquet, C., Vigier, N., Carignan, J. and France-Lanord, C. (2008) Magnesium isotope systematics of the lithologically varied Moselle river basin, France. Geochim. Cosmochim. Acta 72, 5070-5089.

Brey, G.P. and Köhler, T. (1990) Geothermobarometry in four-phase lherzolites II. New thermobarometers, and practical assessment of existing thermobarometers. J. Petrol. 31, 1353-1378.

Clague, D.A. and Frey, F.A. (1982) Petrology and trace element chemistry of the Honolulu volcanics, Oahu: Implication for the oceanic mantle below Hawaii. J. Petrol. 23, 447-504.

512 Dauphas, N., Teng, F.-Z. and Arndt, N.T. (2010) Magnesium and iron isotopes in 2.7 Ga Alexo
513 komatiites: Mantle signatures, no evidence for Soret diffusion, and identification of diffusive
514 transport in zoned olivine. Geochim. Cosmochim. Acta 74, 3274-3291.
515 Dick, H.J.B. and Bullen, T. (1984) Chromian spinel as a petrogenetic indicator in abyssal and alpine-
516 type peridotites and spatially associated lavas. Contrib. Mineral. Petrol. 86, 54-76.
517 Ellis, D.J. and Green, D.H. (1979) An experimental study of the effect of Ca upon garnet-
518 clinopyroxene Fe-Mg exchange equilibria. Contrib. Mineral. Petrol. 71, 13-22.
519 Galy, A., Bar-Matthews, M., Halicz, L. and O'Nions, R.K. (2002) Mg isotopic composition of
520 carbonate: insight from speleothem formation. Earth Planet. Sci. Lett. 201, 105-115.
521 Garcia, M.O., Swinnard, L., Weis, D., Greene, A.R., Tagami, T., Sano, H. and Gandy, C.E. (2010)
522 Petrology, Geochemistry and Geochronology of Kaua'i Lavas over 4-5 Myr: Implications for the
523 Origin of Rejuvenated Volcanism and the Evolution of the Hawaiian Plume. J. Petrol. 51, 1507-
524 1540.
525 George, A.M. and Stebbins, J.F. (1998) Structure and dynamics of magnesium in silicate melts; a high-
526 temperature 25 Mg NMR study. Am. Mineral. 83, 1022-1029.
527 Handler, M.R., Baker, J.A., Schiller, M., Bennett, V.C. and Yaxley, G.M. (2009) Magnesium stable
528 isotope composition of Earth's upper mantle. Earth Planet. Sci. Lett. 282, 306-313.
529 Hin, R.C., Coath, C.D., Carter, P.J., Nimmo, F., Lai, Y.-J., Pogge von Strandmann, P.A.E., Willbold,
530 M., Leinhardt, Z.M., Walter, M.J. and Elliott, T. (2017) Magnesium isotope evidence that accretional
531 vapour loss shapes planetary compositions. Nature 549, 511-515.
532 Hippler, D., Buhl, D., Witbaard, R., Richter, D.K. and Immenhauser, A. (2009) Towards a better
533 understanding of magnesium-isotope ratios from marine skeletal carbonates. Geochim. Cosmochim.
534 Acta 73, 6134-6146.
535 Hu, Y., Teng, F.-Z., Zhang, H.-F., Xiao, Y. and Su, B.-X. (2016) Metasomatism-induced mantle
536 magnesium isotopic heterogeneity: Evidence from pyroxenites. Geochim. Cosmochim. Acta 185,
537 88-111.

538 Huang, F., Chen, L., Wu, Z. and Wang, W. (2013) First-principles calculations of equilibrium Mg
539 isotope fractionations between garnet, clinopyroxene, orthopyroxene, and olivine Implications for
540 Mg isotope thermometry. Earth Planet. Sci. Lett. 367, 61-70.
541 Huang, F., Zhang, Z., Lundstrom, C.C. and Zhi, X. (2011) Iron and magnesium isotopic compositions
542 of peridotite xenoliths from Eastern China. Geochim. Cosmochim. Acta 75, 3318-3334.
543 Kelemen, P.B., Johnson, K.T.M., Kinzler, R.J. and Irving, A.J. (1990) High-field strength element
544 depletions in arc basalts due to mantle-magma interaction. Nature 345, 521-524.
545 Keshav, S. and Sen, G. (2001) Majoritic garnets in Hawaiian Xenoliths: Preliminary results. Geophys.
546 Res. Lett. 28, 3509-3512.
547 Keshav, S., Sen, G. and Presnall, D.C. (2007) Garnet-bearing xenoliths from Salt Lake Crater, Oahu,
548 Hawaii: High-pressure fractional crystallization in the oceanic mantle. J. Petrol. 48, 1681-1724.
549 Li, W.-Y., Teng, F.-Z., Xiao, Y. and Huang, J. (2011) High-temperature inter-mineral magnesium
550 isotope fractionation in eclogite from the Dabie orogen, China. Earth Planet. Sci. Lett. 304, 224-230.
551 Liu, S.-A., Teng, F.-Z., Yang, W. and Wu, F.-Y. (2011) High-temperature inter-mineral magnesium
552 isotope fractionation in mantle xenoliths from the North China craton. Earth Planet. Sci. Lett. 308,
553 131-140.
554 Macris, C.A., Young, E.D. and Manning, C.E. (2013) Experimental determination of equilibrium
555 magnesium isotope fractionation between spinel, forsterite, and magnesite from 600 to 800°C.
556 Geochim. Cosmochim. Acta 118, 18-32.
557 Norman, M.D., Yaxley, G.M., Bennett, V.C. and Brandon, A.D. (2006) Magnesium isotopic
558 composition of olivine from the Earth, Mars, Moon, and pallasite parent body. Geophysical
559 Research Letters 33.
560 Oeser, M., Dohmen, R., Horn, I., Schuth, S. and Weyer, S. (2015) Processes and time scales of
561 magmatic evolution as revealed by Fe–Mg chemical and isotopic zoning in natural olivines.
562 Geochim. Cosmochim. Acta 154, 130-150.
563 Nimis, P. and Grütter, H. (2010) Internally consistent geothermometers for garnet peridotites and
564 pyroxenites. Contrib. Mineral. Petrol. 159, 411-427.

565 Pertermann, M. and Hirschmann, M.M. (2003a) Anhydrous partial melting experiments on a MORB-
566 like eclogite: Phase relations phase compositions and mineral-melt partitioning of major elements at
567 2-3 GPa. J. Petrol. 44, 2173-2201.
568 Pertermann, M. and Hirschmann, M.M. (2003b) Partial melting experiments on a MORB-like
569 pyroxenite between 2 and 3GPa: Constraints on the presence of pyroxenite in basalt source regions
570 from solidus location and melting rate. J. Geophys. Res. 108, 215, doi:210.1029/2000JB000118.
571 Pogge von Strandmann, P.A.E., Burton, K.W., James, R.H., van Calsteren, P., Gislason, S.R. and
572 Sigfússon, B. (2008a) The influence of weathering processes on riverine magnesium isotopes in a
573 basaltic terrain. Earth Planet. Sci. Lett. 276, 187-197.
574 Pogge von Strandmann, P.A.E., Elliott, T., Marschall, H.R., Coath, C., Lai, Y.-J., Jeffcoate, A.B. and
575 Ionov, D.A. (2011) Variations of Li and Mg isotope ratios in bulk chondrites and mantle xenoliths.
576 Geochim. Cosmochim. Acta 75, 5247-5268.
577 Pogge von Strandmann, P.A.E., James, R.H., van Calsteren, P., Gíslason, S.R. and Burton, K.W.
578 (2008b) Lithium, magnesium and uranium isotope behaviour in the estuarine environment of
579 basaltic islands. Earth Planet. Sci. Lett. 274, 462-471.
580 Princivalle, F., Della Giusta, A. and Carbonin, S. (1989) Comparative crystal chemistry of spinels from
581 some suites of ultramafic rocks. Mineralogy and Petrology 40, 117-126.
582 Roeder, P., Campbell, I. and Jamieson, H. (1979) A re-evaluation of the olivine-spinel geothermometer.
583 Contrib. Mineral. Petrol. 68, 325-334.
584 Schauble, E.A. (2011) First-principles estimates of equilibrium magnesium isotope fractionation in
585 silicate, oxide, carbonate and hexaaquamagnesium(2+) crystals. Geochim. Cosmochim. Acta 75,
586 844-869.
587 Schiller, M., Handler, M.R. and Baker, J.A. (2010) High-precision Mg isotopic systematics of bulk
588 chondrites. Earth Planet. Sci. Lett. 297, 165-173.
589 Sedaghatpour, F., Teng, F.-Z., Liu, Y., Sears, D.W.G. and Taylor, L.A. (2013) Magnesium isotopic
590 composition of the Moon. Geochim. Cosmochim. Acta 120, 1-6.

591 Sen, G., Keshav, S. and Bizimis, M. (2005) Hawaiian mantle xenoliths and magmas: Composition and
592 thermal character of the lithosphere. Am. Mineral. 90, 871-887.
593 Sen, I.S., Bizimis, M. and Sen, G. (2010) Geochemistry of sulfides in Hawaiian garnet pyroxenite
594 xenoliths: Implications for highly siderophile elements in the oceanic mantle. Chem. Geol. 273, 180-
595 192.
596 Sen, I.S., Bizimis, M., Sen, G. and Huang, S. (2011) A radiogenic Os component in the oceanic
597 lithosphere? Constraints from Hawaiian pyroxenite xenoliths. Geochim. Cosmochim. Acta 75, 4899-
598 4916.
599 Shaw, D.M. (1970) Trace element fractionation during anatexis. Geochim. Cosmochim. Acta 34, 237-
600 243.
601 Shen, B., Jacobsen, B., Lee, C.-T.A., Yin, Q.-Z. and Morton, D.M. (2009) The Mg isotopic systematics
602 of granitoids in continental arcs and implications for the role of chemical weathering in crust
603 formation. Proceedings of the National Academy of Sciences 106, 20652-20657.
604 Shimoda, K., Tobu, Y., Hatakeyama, M., Nemoto, T. and Saito, K. (2007) Structural investigation of
605 Mg local environments in silicate glasses by ultra-high field 25Mg 3QMAS NMR spectroscopy. Am.
606 Mineral. 92, 695-698.
607 Sio, C.K.I., Dauphas, N., Teng, F.-Z., Chaussidon, M., Helz, R.T. and Roskosz, M. (2013) Discerning
608 crystal growth from diffusion profiles in zoned olivine by in situ Mg–Fe isotopic analyses. Geochim.
609 Cosmochim. Acta 123, 302-321.
610 Stracke, A. and Bourdon, B. (2009) The importance of melt extraction for tracing mantle heterogeneity.
611 Geochim. Cosmochim. Acta 73, 218-238.
612 Teng, F.-Z., Dauphas, N., Huang, S. and Marty, B. (2013) Iron isotopic systematics of oceanic basalts.
613 Geochim. Cosmochim. Acta 107, 12-26.
614 Teng, F.-Z., Li, W.-Y., Ke, S., Marty, B., Dauphas, N., Huang, S., Wu, F.-Y. and Pourmand, A. (2010a)
615 Magnesium isotopic composition of the Earth and chondrites. Geochim. Cosmochim. Acta 74,
616 4150-4166.

617 Teng, F.-Z., Li, W.-Y., Rudnick, R.L. and Gardner, L.R. (2010b) Contrasting lithium and magnesium
618 isotope fractionation during continental weathering. Earth Planet. Sci. Lett. 300, 63-71.
619 Teng, F.-Z., Wadhwa, M. and Helz, R.T. (2007) Investigation of magnesium isotope fractionation
620 during basalt differentiation: Implications for a chondritic composition of the terrestrial mantle.
621 Earth Planet. Sci. Lett. 261, 84-92.
622 Tipper, E.T., Bickle, M.J., Galy, A., West, A.J., Pomiès, C. and Chapman, H.J. (2006a) The short term
623 climatic sensitivity of carbonate and silicate weathering fluxes: Insight from seasonal variations in
624 river chemistry. Geochim. Cosmochim. Acta 70, 2737-2754.
625 Tipper, E.T., Galy, A. and Bickle, M.J. (2006b) Riverine evidence for a fractionated reservoir of Ca and
626 Mg on the continents: Implications for the oceanic Ca cycle. Earth Planet. Sci. Lett. 247, 267-279.
627 Tipper, E.T., Galy, A. and Bickle, M.J. (2008a) Calcium and magnesium isotope systematics in rivers
628 draining the Himalaya-Tibetan-Plateau region: Lithological or fractionation control? Geochim.
629 Cosmochim. Acta 72, 1057-1075.
630 Tipper, E.T., Galy, A., Gaillardet, J., Bickle, M.J., Elderfield, H. and Carder, E.A. (2006c) The
631 magnesium isotope budget of the modern ocean: Constraints from riverine magnesium isotope
632 ratios. Earth Planet. Sci. Lett. 250, 241-253.
633 Tipper, E.T., Louvat, P., Capmas, F., Galy, A. and Gaillardet, J. (2008b) Accuracy of stable Mg and Ca
634 isotope data obtained by MC-ICP-MS using the standard addition method. Chem. Geol. 257, 65-75.
635 Wan, Z., Coogan, L.A. and Canil, D. (2008) Experimental calibration of aluminum partitioning between
636 olivine and spinel as a geothermometer. Am. Mineral. 93, 1142-1147.
637 Wang, S.-J., Teng, F.-Z., Li, S.-G. and Hong, J.-A. (2014) Magnesium isotopic systematics of mafic
638 rocks during continental subduction. Geochim. Cosmochim. Acta.
639 Wang, S.-J., Teng, F.-Z. and Scott, J.M. (2016) Tracing the origin of continental HIMU-like intraplate
640 volcanism using magnesium isotope systematics. Geochim. Cosmochim. Acta 185, 78-87.
641 Wang, S.-J., Teng, F.-Z., Williams, H.M. and Li, S.-G. (2012) Magnesium isotopic variations in cratonic
642 eclogites: Origins and implications. Earth Planet. Sci. Lett. 359–360, 219-226.

643 Wells, P.A. (1977) Pyroxene thermometry in simple and complex systems. Contrib. Mineral. Petrol. 62,
644 129-139.
645 Weyer, S. and Ionov, D.A. (2007) Partial melting and melt percolation in the mantle: The message from
646 Fe isotopes. Earth Planet. Sci. Lett. 259, 119-133.
647 Wiechert, U. and Halliday, A.N. (2007) Non-chondritic magnesium and the origins of the inner
648 terrestrial planets. Earth Planet. Sci. Lett. 256, 360-371.
649 Williams, H.M. and Bizimis, M. (2014) Iron isotope tracing of mantle heterogeneity within the source
650 regions of oceanic basalts. Earth Planet. Sci. Lett. 404, 396-407.
651 Wu, F.-Y., Walker, R.J., Yang, Y.-H., Yuan, H.-L. and Yang, J.-H. (2006) The chemical-temporal
652 evolution of lithospheric mantle underlying the North China Craton. Geochim. Cosmochim. Acta
653 70, 5013-5034.
654 Xiao, Y., Teng, F.-Z., Zhang, H.-F. and Yang, W. (2013) Large magnesium isotope fractionation in
655 peridotite xenoliths from eastern North China craton: Product of melt–rock interaction. Geochim.
656 Cosmochim. Acta 115, 241-261.
657 Yang, W., Teng, F.-Z. and Zhang, H.-F. (2009) Chondritic magnesium isotopic composition of the
658 terrestrial mantle: A case study of peridotite xenoliths from the North China craton. Earth Planet.
659 Sci. Lett. 288, 475-482.
660 Young, E.D. and Galy, A. (2004) The isotope geochemistry and cosmochemistry of magnesium.
661 Reviews in Mineralogy and Geochemistry 55, 197-230.
662 Young, E.D., Tonui, E., Manning, C.E., Schauble, E. and Macris, C.A. (2009) Spinel-olivine magnesium
663 isotope thermometry in the mantle and implications for the Mg isotopic composition of Earth.
664 Earth Planet. Sci. Lett. 288, 524-533.
665 Zhong, Y., Chen, L.-H., Wang, X.-J., Zhang, G.-L., Xie, L.-W. and Zeng, G. (2017) Magnesium
666 isotopic variation of oceanic island basalts generated by partial melting and crustal recycling. Earth
667 Planet. Sci. Lett. 463, 127-135.
668
669

Figure and Table captions:

Fig. 1: $\delta^{26}Mg$ values in minerals from the Hawaiian spinel peridotite (olivine, orthopyroxene, clinopyroxene, spinel) and garnet pyroxenite (garnet, clinopyroxene) xenoliths investigated in this study (colored symbols) compared to $\delta^{26}Mg$ values in minerals from peridotites and eclogites reported in the literature (gray symbols). Literature data are from (Handler et al., 2009; Huang et al., 2011; Li et al., 2011; Liu et al., 2011; Pogge von Strandmann et al., 2011; Wang et al., 2014; Wang et al., 2016; Wang et al., 2012; Wiechert and Halliday, 2007; Xiao et al., 2013; Yang et al., 2009; Young et al., 2009).

Fig. 2: Inter-mineral fractionation factors $\Delta^{26}Mg_{X-Y} = \delta^{26}Mg_X - \delta^{26}Mg_Y$ for minerals from Hawaiian spinel peridotites (olivine, orthopyroxene, clinopyroxene, spinel) and garnet pyroxenites (garnet, clinopyroxene) (colored symbols) compared to $\Delta^{26}M\ g_{X-Y}$ values in minerals from spinel peridotites and eclogites reported in the literature (gray symbols). Literature data are from (Handler et al., 2009; Huang et al., 2011; Li et al., 2011; Liu et al., 2011; Pogge von Strandmann et al., 2011; Wang et al., 2014; 2016; 2012; Wiechert and Halliday, 2007; Xiao et al., 2013; Yang et al., 2009; Young et al., 2009).

Fig. 3: a) Diagram showing $\Delta^{26}Mg_{olivine\text{-}spinel}$ versus Cr# in spinel, and **b)** $\Delta^{26}Mg_{olivine\text{-}spinel}$ versus $10^6/T^2_{BKN}$ for the peridotites with reported Mg isotope ratios in spinel. The Cr# is the molar ratio Cr/(Cr+Al), Mg# is the molar ratio $Mg/(Mg+Fe^{2+})$, and T_{BKN} is the Mg-Fe exchange temperature between clino- and orthopyroxene, estimated after Brey and Köhler (1990) for an assumed equilibration pressure of 15 kb, and $\Delta^{26}Mg_{olivine\text{-}spinel} = |(\delta^{26}Mg_{ol} - \delta^{26}Mg_{sp})|$. There is no systematic decrease in $\Delta^{26}Mg_{olivine\text{-}spinel}$ with Cr# in spinel, as would be expected based on theoretical predictions for refractory peridotites, nor a systematic relation between $\Delta^{26}Mg_{cpx\text{-}grt}$ and $10^6/T^2_{BKN}$, suggesting that secondary processes (post-melting metasomatism) have disturbed these predicted primary relations. Gray lines are drawn using predictions by Schauble, (2011) and Macris et al., (2013). The $\Delta^{26}Mg_{olivine\text{-}spinel}$ for peridotites

696 with different Cr# are linearly interpolated between the predicted $\Delta^{26}Mg_{olivine\text{-}spinel}$ for pure $MgCr_2O_4$
697 and $MgAl_2O_4$ (Schauble, 2011; Macris et al., 2013). Note that there is an offset between the
698 temperatures inferred for $\Delta^{26}Mg_{olivine\text{-}spinel}$ from theoretical models (Schauble, 2011, Macris et al.,
699 2013) and Mg-Fe exchange equilibria in pyroxenes (T_{BKN}, Brey and Köhler; 1990). Error bars for
700 $\Delta^{26}Mg_{olivine\text{-}spinel}$ are drawn assuming an uncertainty of ± 0.10‰ (2 S.D.) on $\delta^{26}Mg_{ol}$ and $\delta^{26}Mg_{sp}$, and
701 thus a propagated uncertainty on $\Delta^{26}Mg_{ol\text{-}sp}$ of ± 0.14‰ (2 S.D.) for all samples. Data and
702 references for the major element data are given in the supplementary data.
703
704 **Fig. 4:** Diagram showing **a)** Cr# in spinel versus Mg# in olivine, and **b)** Al_2O_3 (wt.%) in the whole rock
705 versus Mg# in olivine for the peridotites with reported Mg isotope ratios in spinel. For peridotites
706 with a simple history of depletion by partial melting, a positive correlation in Fig. 4a and a negative
707 correlation in Fig. 4b would be expected. With the possible exception of the peridotites investigated
708 by Liu et al. (2011), the lack of such correlations indicate that the investigated peridotite suites are
709 affected by post-melting melt-rock reaction (metasomatism, see also Fig. 4). Further explanations are
710 given in the main text. Data and references for the major element data are given in the
711 supplementary data.
712
713 **Fig. 5:** Diagram showing $\Delta^{26}Mg_{cpx\text{-}grt}$ versus temperatures estimated based Fe-Mg exchange (Ellis and
714 Green, 1979). The gray curves show the $\Delta^{26}Mg_{cpx\text{-}grt}$ – T parameterization of Huang et al. (2013) for
715 pressures between 2 and 5 GPa. The Hawaiian pyroxenites equilibrated at a mean pressure of ~2.5
716 GPa (Bizimis et al., 2005), the pressure of equilibration for the data from Li et al. (2011) is 3 GPa
717 and 5 GPa for the eclogites studied by Wang et al. (2012). Data from Hu et al. (2016) are omitted,
718 because their clinopyroxene–garnet isotope ratios indicate isotopic disequilibrium.
719
720 **Fig. 6:** Diagram showing the deviation in $\delta^{26}Mg$ of instantaneous and accumulated melts and residue
721 from the initial source composition for melting spinel peridotite (MORB), garnet peridotite (OIB),

and garnet pyroxenite. F is the extent of melting, i.e., the mass of melt generated relative to the mass of the source. The δ^{26}Mg of the partial melts become different form their source value owing to the changing contribution of Mg from the different source minerals to the melt. Garnet has a large influence on the δ^{26}Mg of the partial melt, but the calculated variation in δ^{26}Mg is small (~ 0. 03‰) relative to the typical analytical uncertainty of ~ 0.1‰. Note that $\alpha_{mineral\text{-}melt}$ used in the calculations are calculated from known inter-mineral isotope fractionation factors (Fig. 2) and assuming an initial $\alpha_{source\text{-}melt} = 1$, hence the calculated deviations from the initial source are minimum deviations, and the overall offset to the initial source could be larger for any initial $\alpha_{source\text{-}melt} \neq 1$. Further details of the partial melting calculations are described in the text and the supplementary information.

Fig. 7: Observed variation between bulk rock δ^{26}Mg and Sm/Yb in OIB and MORB. Data are grouped in (1) OIB from the South Pacific and South Atlantic, which are created by small amounts of melting in the garnet stability field (colored circles), (2) OIB created by large amounts of melting in the garnet stability field with intermediate Sm/Yb (Hawaii, diamonds), and (3) ridge basalts (squares) including those from Iceland (green squares), which are dominated by melting in the spinel stability field with Sm/Yb ~ 1 (Fig. 7c). The Mg isotope data are taken from ref. 1: Bourdon et al. (2010), ref. 2: Teng et al. (2010a), and Zhong et al. (2017). Data and references for the trace element data are given in the supplementary data.

Figure 1

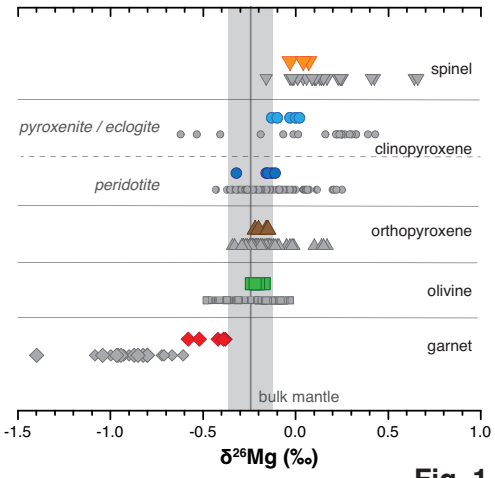

Fig. 1

Figure 2

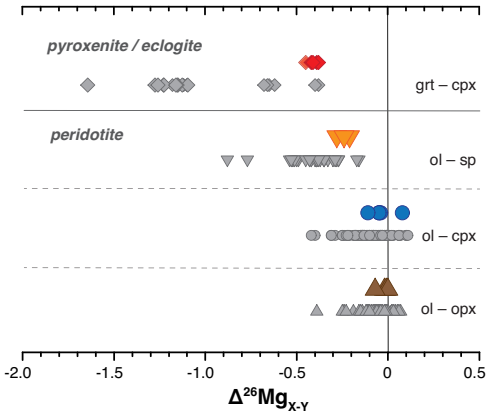

Fig. 2

Figure 3

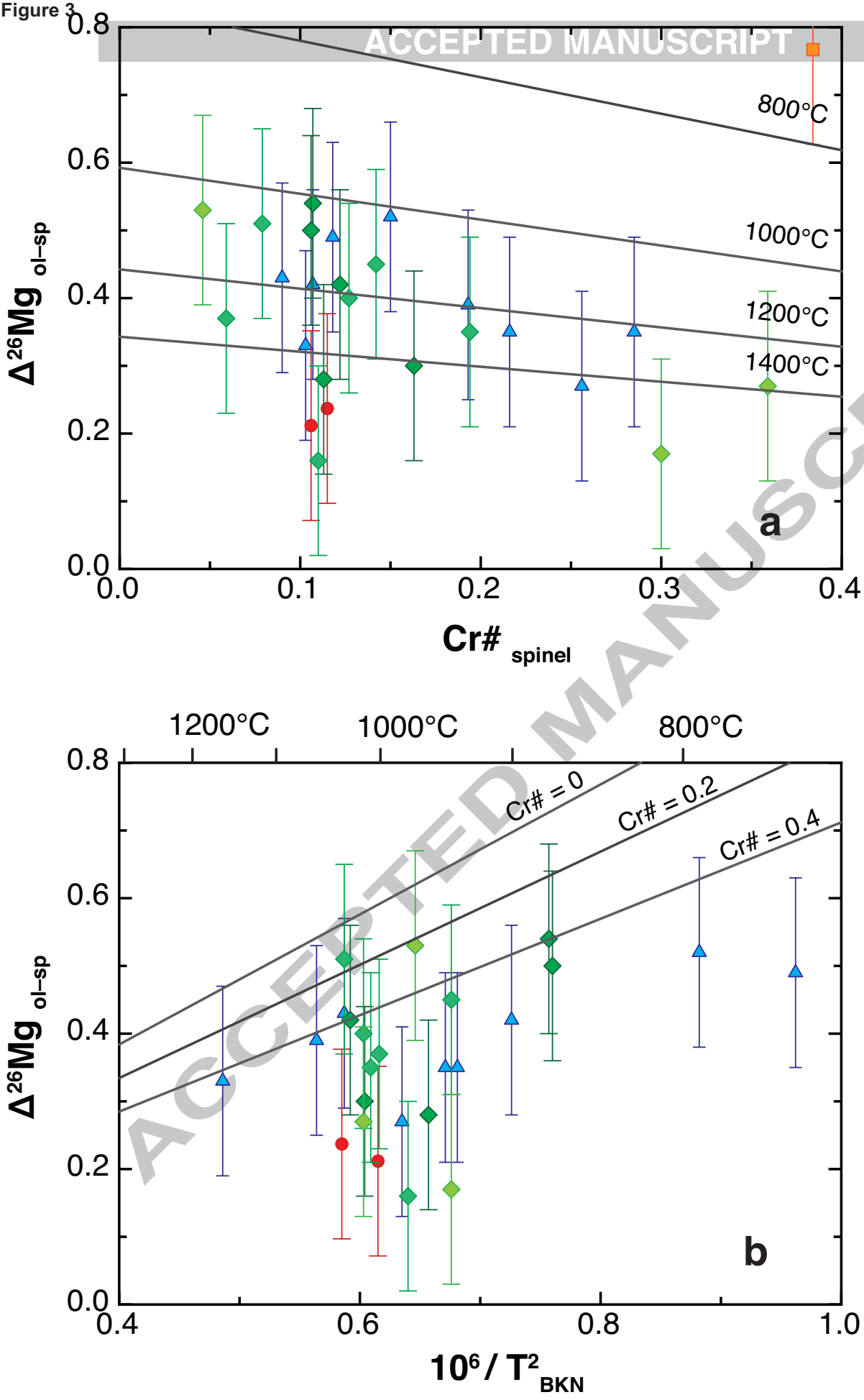

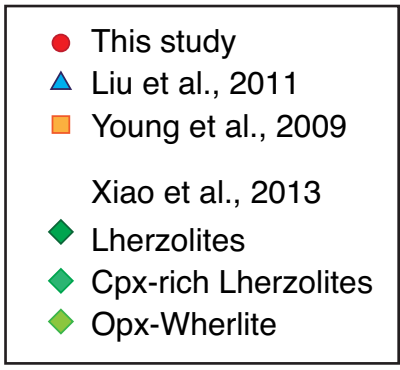

Fig. 3

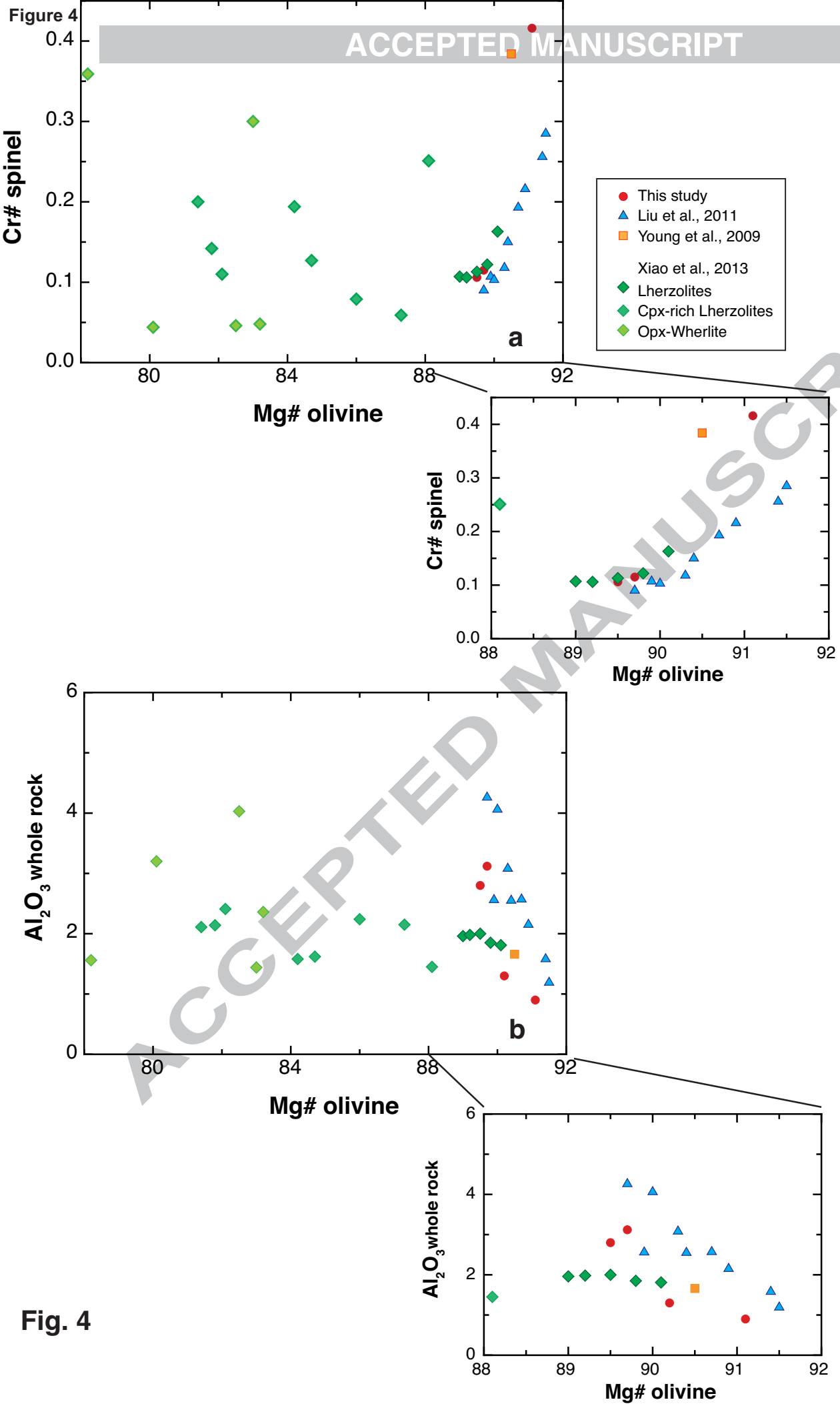

Figure 4

Fig. 4

Figure 5

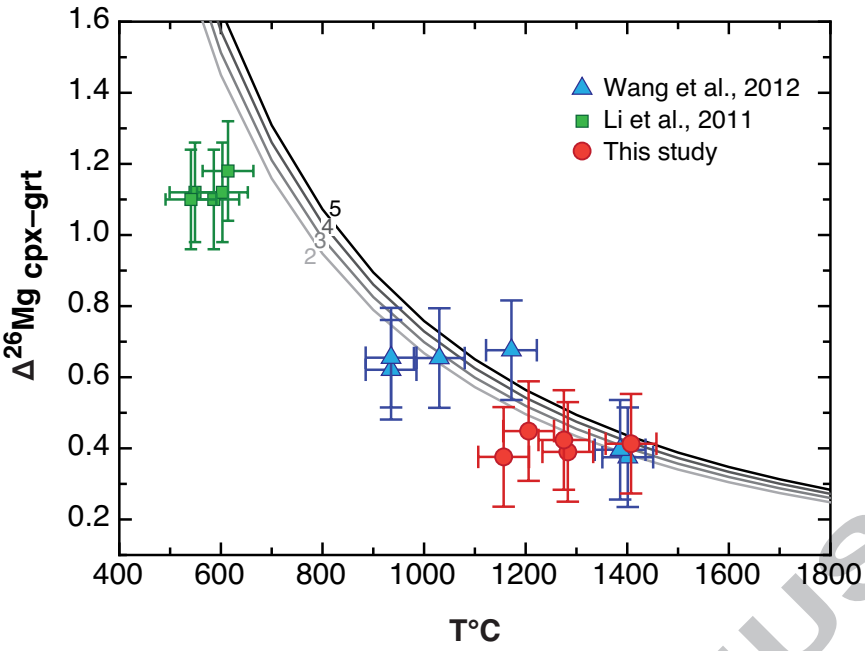

Fig. 5

Figure 6

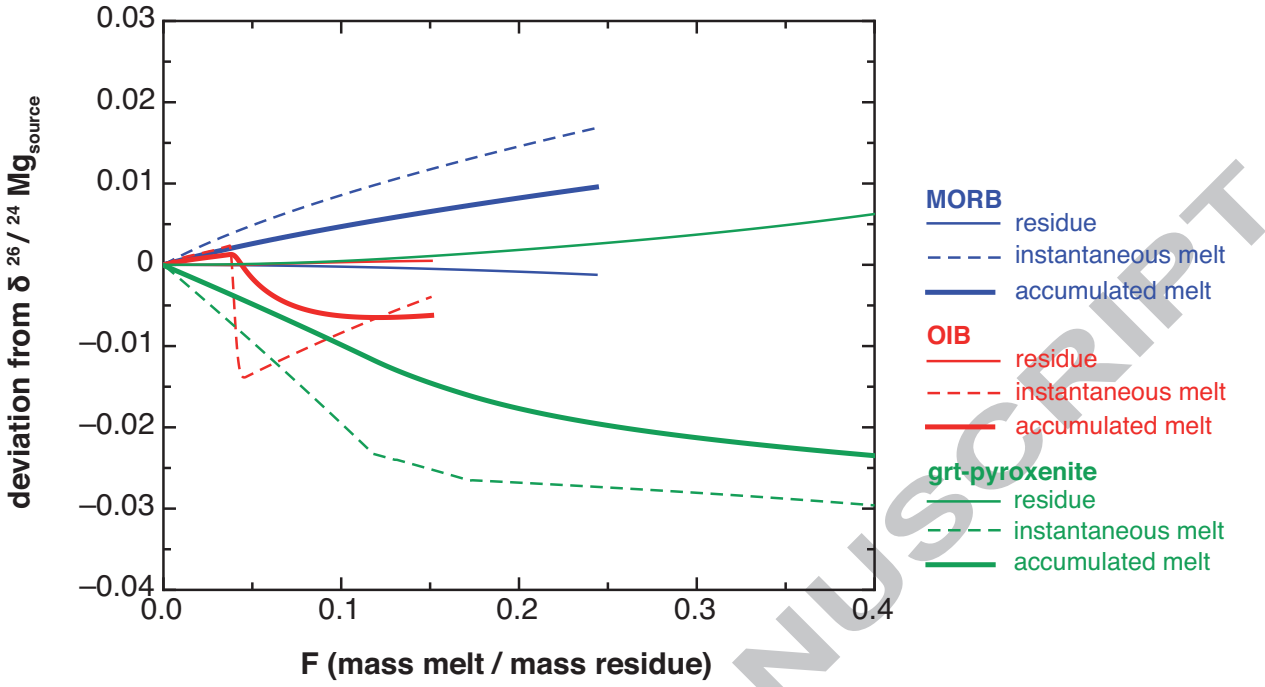

Fig. 6

Figure 7

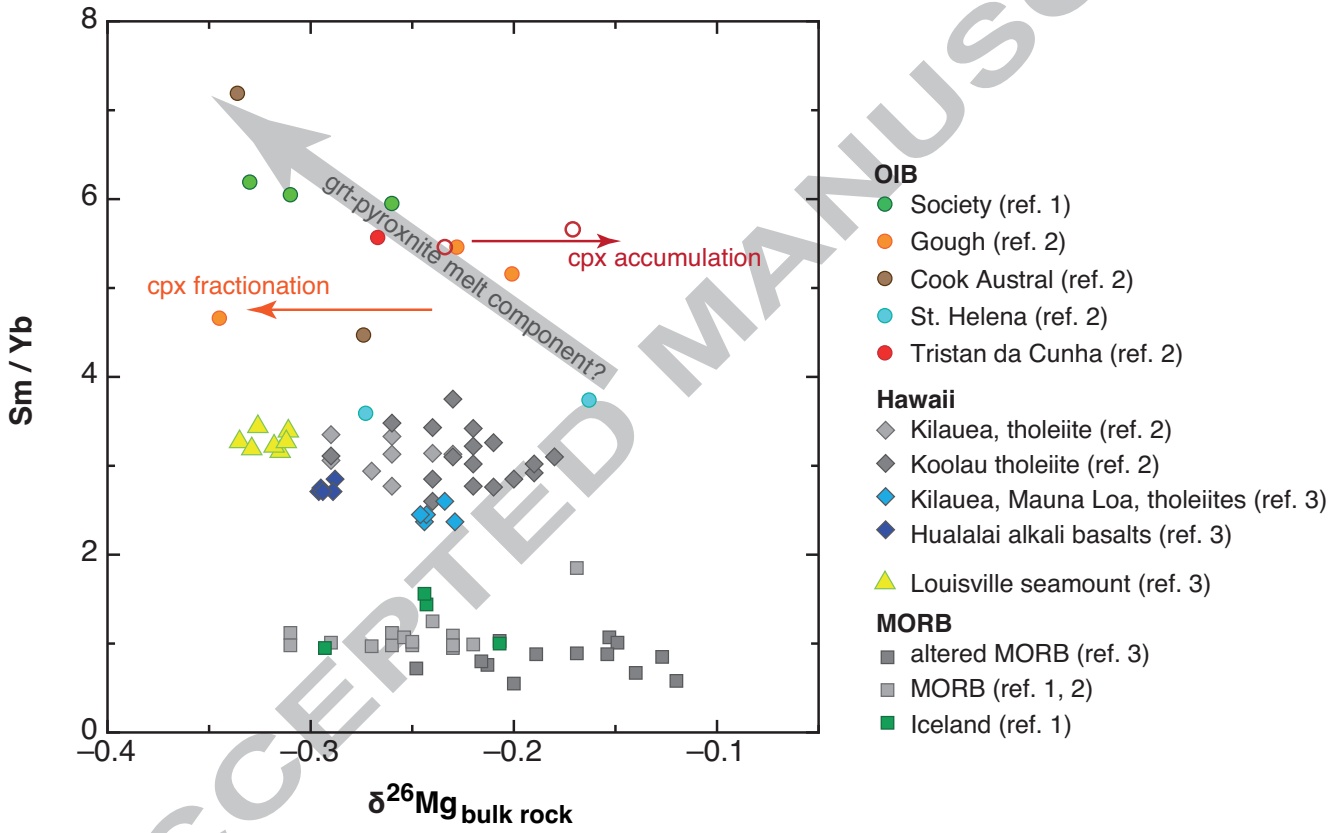

Fig. 7

Figure 1 supplement

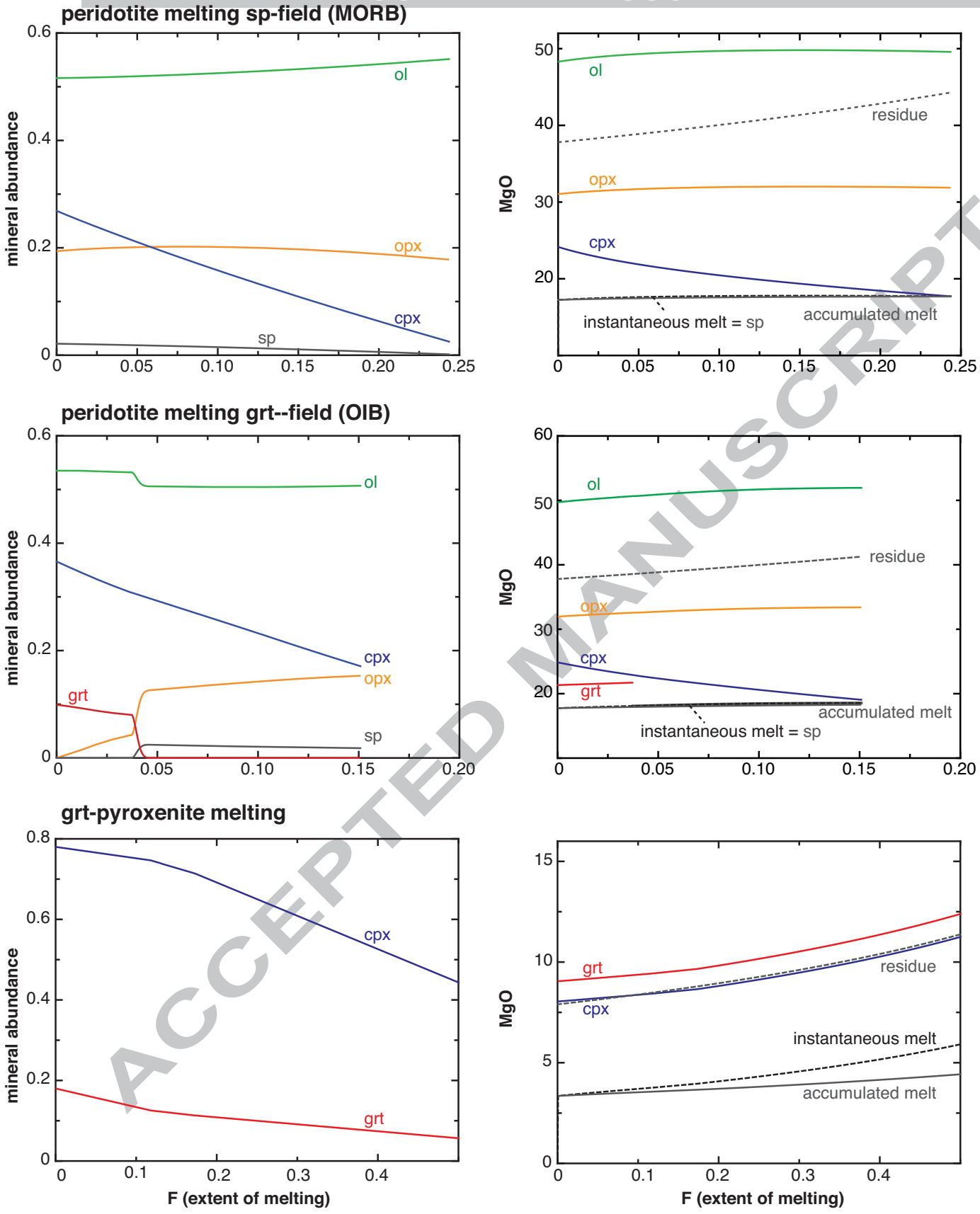

supplementary Fig. 1

Figure 2 supplement

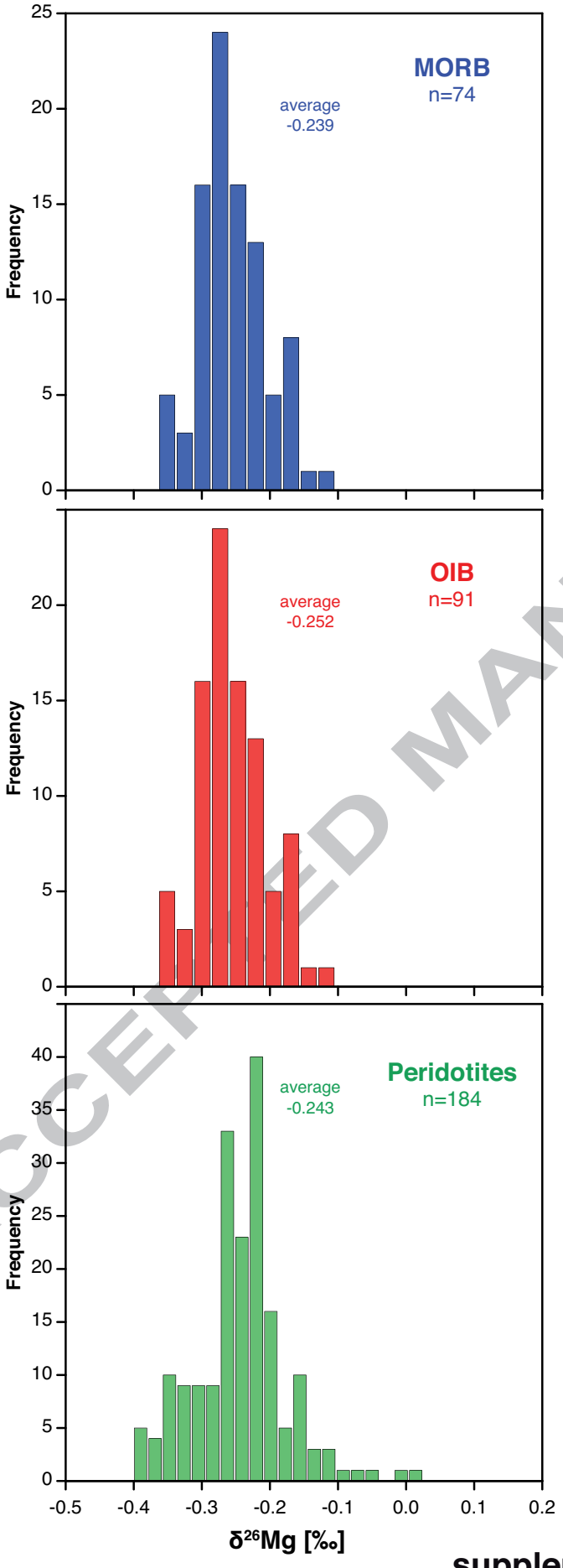

supplementary Fig. 2